*Rock Dynamics – Experiments, Theories and Applications – Li, Li & Zhang (Eds)*
*© 2018 Taylor & Francis Group, London, ISBN 978-0-8153-9667-3*

# Numerical simulations on failure and stress wave propagation in solid materials using a 3D lattice spring model

T. Nishimura & M. Kohno
*Tottori University, Tottori, Japan*

K. Fumimura
*Taisei Cooperation, Tokyo, Japan*

ABSTRACT: A three-dimensional numerical model, in which matter is discretized into a system of mass points connected with springs, is developed for the study of rocks. This model applies to two dynamic problems: one is stress concentration and failure initiation at a crack tip in plate subjected to a uniform tension and the second is a wave propagation problem in plate. The first numerical example represents the value of the stress intensity factor calculated by the linear elastic fracture theory. The stress state reaches the limitation (tensile strength), then tensile failure surface initiates at the tip. The failure surface is progressively developed and the rate of the development is deeply related to the value of the damping constant in the equation of motion. The second is the propagation of plane harmonic wave. Directional characteristics for the wave through the two lattice structures are displayed.

## 1 INTRODUCTION

On the macroscopic level of observation, rock can be seen as a thing consisting of a number of different and distinct particles are adhesively interacting as a result of micro-structural forces. With such a representation, the modelling of the mechanical behavior of rock materials may be generally divided into two categories. Firstly, there are the discrete models, for which the equilibrium conditions, the kinematic conditions and the constitutive behavior are formulated for each individual micro-structural element with respect to its neighboring micro-structural elements. Secondly, there are the continuum models, where the equilibrium conditions, the kinematic conditions and the constitutive behavior are formulated for an assembly of micro-structural elements, using the continuum concepts of stress and strain. A considerable advantage of discrete models in comparison to continuum models is that the inhomogeneous effect at the micro-level can be taken into account more accurately and the dynamic failure process can be properly described. However, the relation between representative micro-structural elements in a macro-structural configuration has yet to be developed, which causes the discrete models to embody the procedure to get the relation between the micro-structural parameters and the macro properties, such as Young's modulus and Poisson's ratio.

A three-dimensional numerical model, in which matter is discretized into a system of mass points connected with springs, is developed for the study of rocks. The relationships between the micromechanical parameters of the springs and the macro material elastic constants of the matter have been derived and the explicit finite difference scheme is adopted for solving the system of the equations of motion (Nishimura et. al. 2014). The local strains are evaluated by the relative normal and shear displacement vectors between particles. It is known that the rigid rotation should not produce strain energy. Therefore, in this method, the rotation related term is expressed with the Euler angle and is removed from the calculation of the relative shear displacement vector. The stress state is evaluated on each nodal point and failure can be examined based on a failure criterion.

In this paper, this model applies to two dynamic problems: one is stress concentration and failure initiation at a crack tip in plate subjected to a uniform tension and the second is a wave propagation problem in plate. The first numerical model represents the value of the stress intensity factor calculated by the linear elastic fracture theory. The stress state reaches the limitation (tensile strength), then tensile failure surface initiates at the tip. The failure surface is progressively developed and the rate of the development is deeply related to the value of the damping constant in the equation of motion. The second is prepared to simulate the propagation of plane harmonic wave using two different lattice structures. Directional characteristics for the wave propagation through the both lattice structures are displayed. This model will be examined by numerical tests before being applied to any case study in this paper.

## 2 DISTINCT ELEMENT MODELING FOR ELASTICITY

### 2.1 *Physical model and the equation of motion*

The body to be analyzed is divided into small portions and is represented by a system of points linked together with the neighboring points as shown Figure 1. The particles and bonds form a network system representing the material. For this system, the equation of motion can be expressed as

$$\mathbf{m}\ddot{\mathbf{u}} + \mathbf{c}\dot{\mathbf{u}} + \mathbf{k}\mathbf{u} = \mathbf{f} \tag{1}$$

where **u** represents the vector of particle displacement, **k** is the stiffness, **m** is the mass matrix, **c** is the damping matrix and **f** is the vector of external force. Equation (1) is solved by using the explicit finite difference scheme.

$$\ddot{\mathbf{u}}_t = \frac{1}{\mathbf{m}}\left[\mathbf{f} - \mathbf{c}\dot{\mathbf{u}}_t - \mathbf{k}\mathbf{u}_t\right] \tag{2}$$

The displacement of particle at time $t{+}\Delta t$ can be expressed as

$$\Delta\mathbf{u}_t = \Delta\mathbf{u}_{t-\Delta t} + \ddot{\mathbf{u}}_t \Delta t^2 \tag{3}$$

where $\Delta\mathbf{u}_t = \mathbf{u}_{t+\Delta t} - \mathbf{u}_t$. The new position of particle is also expressed as

$$\mathbf{u}_{t+\Delta t} = \mathbf{u}_t + \dot{\mathbf{u}}_t \Delta t + \ddot{\mathbf{u}}_t \Delta t^2/2 \tag{4}$$

The particle velocity at $t$ is given by

$$\dot{\mathbf{u}}_t = \frac{\mathbf{u}_t - \mathbf{u}_{t-\Delta t}}{\Delta t} + \ddot{\mathbf{u}}_t \Delta t/2 \tag{5}$$

To keep the computation stable, the time step could be chosen as

$$\Delta t < \min\left(\frac{d_0}{c_{\mathrm{p}}}\right) \tag{6}$$

where $d_0$ is the contact length, that is the distance between particles, and $c_{\mathrm{p}}$ is the P-wave velocity. For static simulation, the equations of motion are damped to reach an equilibrium state under given boundary conditions as quickly as possible. In this modeling, the damping effect is incorporated as written in the following.

$$\ddot{\mathbf{u}}_t = \frac{1}{\mathbf{m}}\left(\sum \mathbf{f}_t - \mathrm{sgn}(\dot{\mathbf{u}}_{t-\Delta t}) \cdot \alpha \left|\sum \mathbf{f}_t\right|\right) \tag{7}$$

where $\alpha$ is the damping constant which is independent of mechanical properties of the material.

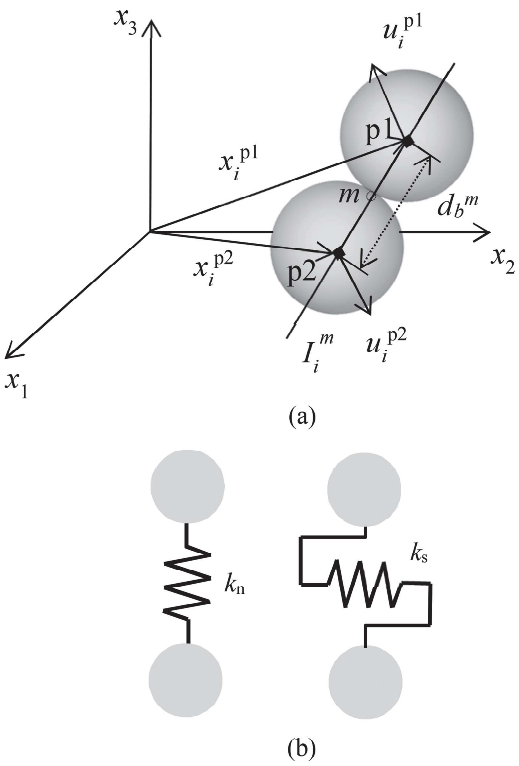


Figure 1. Modeling of the material: (a) linkage of two points and coordinates system and (b) the normal and tangential springs.

### 2.2 *Relating spring stiffness to the elastic properties*

We assume that the medium is loaded from zero condition to an initial condition defined by the strain $e_{ij}$ and the stress $\sigma_{ij}$. For such a system, one can write the displacement for a particle (or element) p with position $x_i$ as follows

$$u_i^{\mathrm{p}} = e_{ij} x_j^{\mathrm{p}} \tag{8}$$

where $e_{ij}$ should be a symmetric tensor which is calculated by removing an asymmetric tensor from the displacement-gradient tensor. The rotation-related term is removed from the relative translational displacement between these two points, then this method ensures that the calculated strain is independent of rotational displacement (Nishimura et. al. 2014).

The following contact law, which relates normal and shear forces $F_{(n)}$, $F_{(s)}$ to normal and shear relative displacements $U_{(n)}$, $U_{(s)}$ holds at the contact

$$F_{(n)} = k_n U_{(n)}, \quad F_{(s)} = k_s U_{(s)} \tag{9}$$

Let us assume that a contact $m$ connects two particles p1 and p2 (see Figure 1), then the normal and shear relative displacements can be written as

$$U_{(n)}^m = \Delta u_i^m I_i^m \tag{10}$$

$$U_{(s)i}^m = \Delta u_i^m - U_{(n)}^m I_i^m \tag{11}$$

where the relative displacement at the contact $\Delta u_i^m$ is given as

$$\Delta u_i^m = e_{ij}\left(x_j^{p1} - x_j^{p2}\right) = e_{ij} d_b^m I_j^m \tag{12}$$

where $I_i^m$ is the normal unit vector. The total force $f_i$ at contact $m$ can be written as

$$\begin{aligned} f_i^m &= k_n^m \Delta u_j^m I_j^m I_i^m + k_s^m\left(\Delta u_i^m - \Delta u_j^m I_j^m I_i^m\right) \\ &= \left(k_n^m - k_s^m\right)\left(e_{kl} I_k^m I_l^m\right) I_i^m d_b^m + k_s^m e_{ij} I_j^m d_b^m \end{aligned} \tag{13}$$

Notice that Einstein summation convention with dummy subscript $i$, $j$, $k$, $l$ is used in the preceding equations. The total strain energy stored per unit volume is

$$\Pi = \frac{\Pi_b}{V} = \frac{1}{V}\sum_{m=1}^{N_c}\frac{1}{2}\left(e_{ij} d_b^m I_j^m f_j^m + e_{ji} d_b^m I_i^m f_i^m\right) \tag{14}$$

where $N_c$ is the number of contacts inside the medium, $V$ is the medium volume. The stress tensor of the continuum can be obtained through the classical elastic theory, and it can be written as (assuming symmetrical stress) (Walton 1987, Richard & Leo 1988).

$$\sigma_{ij} = \frac{1}{2V}\sum_{m=1}^{N_c}\left(d_b^m I_i^m f_j^m + d_b^m I_j^m f_i^m\right) \tag{15}$$

From Equations (13) and (15), we end up with

$$\begin{aligned} \sigma_{ij} = \frac{1}{V}\sum_{m=1}^{N_c}\frac{1}{2}\Big(& k_s^m e_{jl} I_l^m I_i^m d_b^{m2} + k_s^m e_{il} I_l^m I_j^m d_b^{m2} \\ &+ \left(k_n^m - k_s^m\right) e_{kl} I_i^m I_j^m I_k^m I_l^m d_b^{m2}\Big) \end{aligned} \tag{16}$$

The constitutive matrix $C_{ijkl}$ in the classical elasticity theory is expressed as

$$\sigma_{ij} = C_{ijkl} e_{kl} \tag{17}$$

and finally, by substituting Equation (17) into Equation (16), $C_{ijkl}$ can be given as

$$\begin{aligned} C_{ijkl} = \frac{1}{V}\sum_{m=1}^{N_c}\Big(& \frac{k_s^m d_b^{m2}}{4}\left(I_j^m I_k^m \delta_{il} + I_i^m I_k^m \delta_{jl} + I_j^m I_l^m \delta_{ik} + I_i^m I_l^m \delta_{jk}\right) \\ &+ \left(k_n^m - k_s^m\right) d_b^{m2} I_i^m I_j^m I_k^m I_l^m\Big) \end{aligned} \tag{18}$$

where $\delta_{ij}$ is the Kronecker's delta. Then, the relationship the micro-mechanical parameters $k_n$, $k_s$ and the macro material constants the Young' modulus $E_0$ and the Poisson's ratio $\nu_0$ can be obtained by comparing Equation (18) to the classical elastic matrix. As seen in this equation, the values of the stiffness are influenced by the normal unit vector, therefore, the lattice structure should be carefully modeled.

## 3 NUMERICAL EXAMPLES

### 3.1 *Plate subjected to uniform tension*

Brittle process is often observed in deformation and failure of rock. Numerical methods and techniques have been proven as a powerful tool to study rock mechanical characteristics. In this paper, this numerical model applies to two dynamic problems: one is stress concentration and failure initiation at a crack tip in plate subjected to a uniform tension and the other is a wave propagation problem in plate. Two lattice geometries are prepared: a 6-bond cubic lattice and an 18-bond cubic lattice as shown in Figure 2.

One problem with Type 1 is that this structure shows a Poisson's ratio equals to 0, which makes it impractical to model real rock-like materials. This

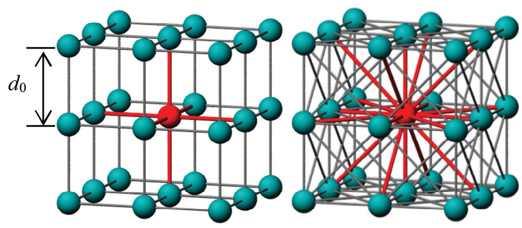


Figure 2. Two different structures of spring linkage: (a) 6-bond model and (b) 18-bond model.

problem is solved by introducing a diagonal interaction between particles. Using Equation (18), for Type 2, the micro-mechanical parameters $k_n$, $k_s$ are obtained by

$$k_n = \frac{E_0 d_0}{5(1-2\nu_0)} \tag{19}$$

$$k_s = \frac{(1-4\nu_0)E_0 d_0}{5(1+\nu_0)(1-2\nu_0)} \tag{20}$$

Equation (20) shows that the spring stiffness of negative occurs when $\nu_0$ is greater than 0.25. For this condition, the numerical model shown in Figure 4(a) indicates unstable behavior and never reaches the quasi-static state under a given static boundary condition. Therefore, numerical results shown in this paper will be carried out for $\nu_0 < 0.25$. This negative effect of the Poisson's ratio in such lattice modeling has also been reported (e.g. Zhao et al. 2011).

Figure 3(a) shows a problem of stress concentration and failure initiation at a crack tip in a plate subjected to a uniform tension. Figure 3(b) is the numerical model with $W_0 = 7.1$ cm, $L_0 = 14.1$ cm and a crack of 0.1 cm in width. Figure 4 shows the schematic view of numerical results for stress distribution of $\sigma_y$. In Figure 4(a), the radius of the particle is 0.1 cm and the total number of particles

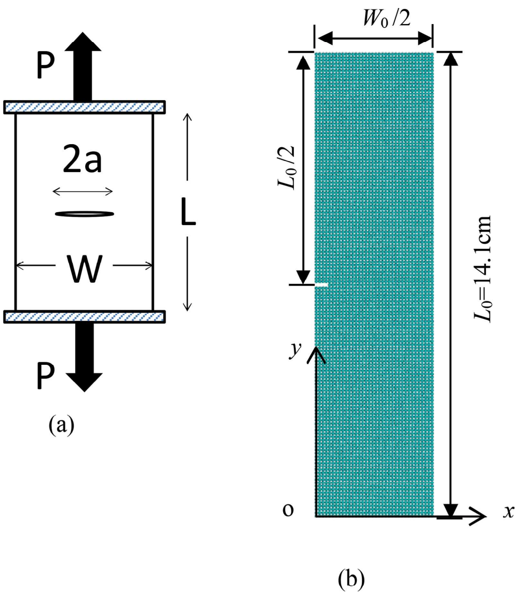


Figure 3. Problem of stress concentration and failure initiation at a crack tip in a plate subjected to a uniform tension (a) and numerical model using the lattice structure (b).

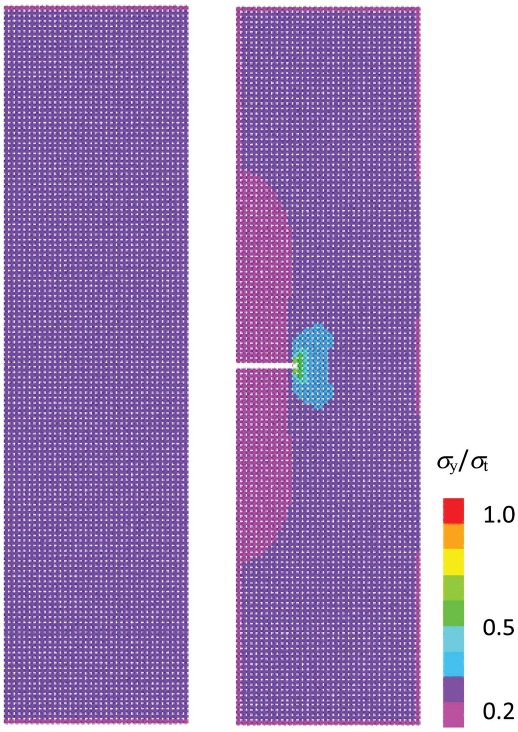


(a) $a$=0 (b)$2a/W$=0.3

Figure 4. Numerical results of the plate model subject to uniform tension without/with the crack. In figure (b), the crack width is 0.1 cm.

Table 1. Numerical results of the stress intensity factor and the tensile force, comparing with the values obtained by of the linear elastic fracture theory.

| | $K_I \Big/ \left( \frac{P_0\sqrt{\pi W}}{WT} \right)$ | | $P_y/P_0$ | |
|---|---|---|---|---|
| $2a/W$ | Type 2 | error (%) | Type 2 | error (%) |
| 0.1 | 0.238 | 0.4 | 0.989 | 0.3 |
| 0.3 | 0.390 | 0.7 | 0.923 | 0.8 |
| 0.5 | 0.477 | 0.6 | 0.802 | 0.6 |
| 0.7 | 0.571 | 1.0 | 0.630 | 1.5 |

is 55836 ( = 36 × 141 × 11). Type 2 is selected as the structures of spring linkage in this simulation. The Young's modulus and the Poisson's ratio are set 1000 MPa and 0.2 respectively. The stress concentration is found at/around the crack tip in Figure 4(b). Table 1 lists the values of the stress intensity factor obtained from the numerical analysis, in which $P_y$ is the tensile force acting on the plate with the crack and $P_0$ is also the tensile force acting on the plate of $a = 0$ in $y$ direction. Based on the linear elastic fracture theory, the theoretical value of the stress intensity factor is given by (Okamura 1976)

$$K_1 = \frac{P_y\sqrt{\pi a}}{WT}\sqrt{\sec\frac{\pi}{2}\frac{2a}{W}} \tag{21}$$

$$P_y \big/ P_0 = \frac{1}{1+\kappa\beta\Gamma\left(\frac{2a}{W}\right)} \tag{22}$$

$$\text{where} \quad \Gamma\left(\frac{2a}{W}\right) = \pi\int_0^{2a/W}\xi\sec\frac{\pi\xi}{2}d\xi \tag{23}$$

$\kappa\beta$ is a value which is related to the boundary condition and the value of $W/L$ and is set 0.5 in this analysis. Agreement can be recognized between the numerical results and the theoretical values calculated by the theory. For these static analyses listed in Table 1, the value of the damping constant appeared in Equation (7) is set 0.8.

The tensile strength of the plate is set $\sigma_t = 8$ MPa and the development of the tensile failure surface is simulated. The time increment written in Equation (6) is set $\Delta t = 10^{-8}$ sec. Figure 5 shows the numerical results at time $t = 10^{-4}$ sec. For dynamic case, the damping term is often neglected (i.e. $\alpha = 0$) and the released elastic strain energy is fully transformed into the kinetic energy of nodes surrounding the failure surface. In this analysis, numerical trials have been executed with several values of the damping constant to learn the effect of the factor on the development of the failure surface and the numerical stability. Figure 5 shows that the value of the damping constant should be carefully selected to simulate the development of the failure surface using this numerical procedure.

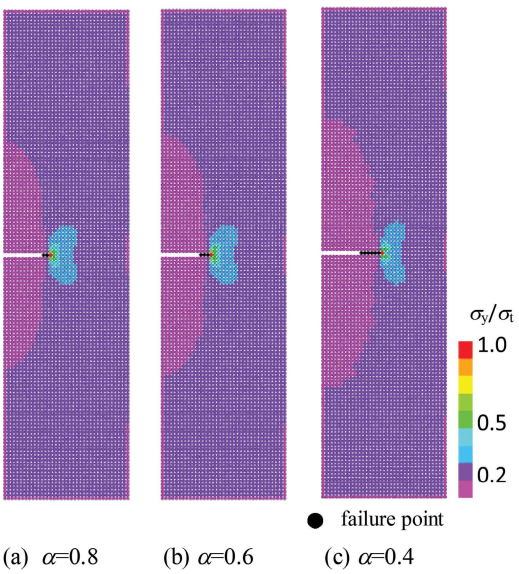


Figure 5. Schematic numerical results for stress distribution of $\sigma_y$ and tensile crack development in the computation of the plate for three values of the damping constant.

To compare the dynamic behavior of the two lattice structures, we will analyze the propagation of plane harmonic waves. For this wave type, the displacements ($u_x$, $u_y$) at position ($x$, $y$) have form

$$u_x = A\exp(i(\omega t - k_x x - k_y y)) \tag{24}$$

$$u_y = B\exp(i(\omega t - k_x x - k_y y)) \tag{25}$$

where $\omega$ is the angular frequency of the wave, $A$ and $B$ are the wave amplitudes and $k_x$ and $k_y$ are the wave numbers in the $x$ direction and $y$ direction, respectively. The vector of wave numbers $\mathbf{k} = (k_x, k_y)$ is related to the vector of wavelength $\mathbf{\Lambda} = (\lambda_x, \lambda_y)$ with the scalar product $\mathbf{k}\bullet\mathbf{\Lambda} = 2\pi$ and the vector of wave numbers is related to the vector of velocities $\mathbf{c} = (c_x, c_y)$, $\mathbf{k}\bullet\mathbf{c} = \omega$.

Figure 6 shows the two-dimensional representation of the lattice models used in the compression wave propagation simulation. As seen in Figure 6, the circular area is used for this simulation and wave propagates only in $x$-$y$ plane. The elastic properties of the material are $E_0 = 50$ MPa, $v_0 = 0.2$. The area is 30 cm in radius and is discretized with enough number of particles in radial direction to express the wavelength. The radius of the particle is 2 mm and the total number of particles is 70681. Figure 6 gives the input conditions where $A = B = 1.0 \times 10^{-3}$ cm.

Figure 7 shows the directional characteristics for the compression wave propagating through

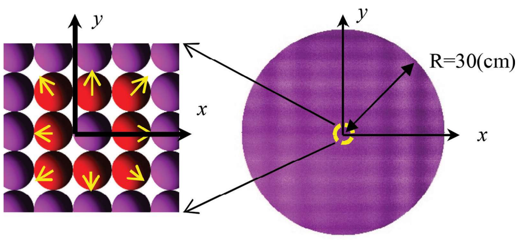


Figure 6. Two-dimensional representation of the lattice models used in the compression wave propagation simulation.

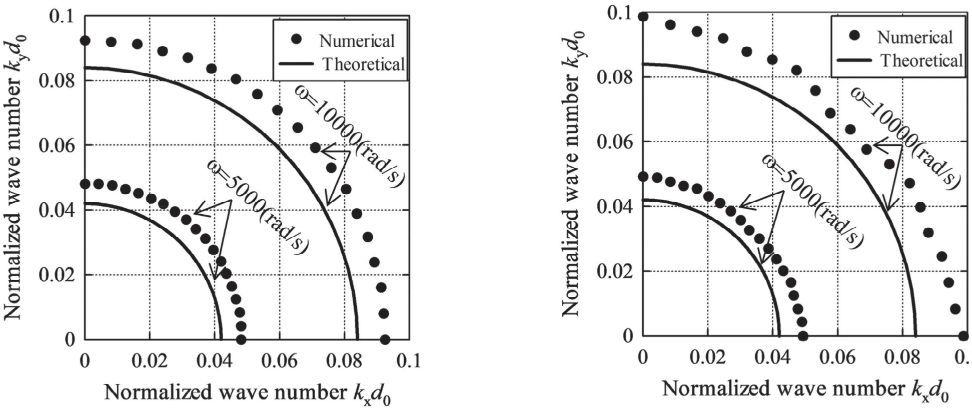


(a)Type 1 (b) Type 2

Figure 7. Directional characteristics for the compression wave propagating through the lattice structure; the normalized wave number $k_x d_0$ versus the normalized wave number $k_y d_0$ for two different frequencies.

the lattice structure where the normalized wave number $k_x d_0$ versus the normalized wave number $k_y d_0$ for two different frequencies. From these two figures, it can be recognized that the numerical results for Type 1 are plotted in a circular shape of $k_x$-$k_y$ curves and the curves of Type 2 loses circularity. The difference in the two lattice structures is the diagonal springs and this may cause the reduction of the wave number in diagonal direction in Type 2. It must be concluded that the lattice model should carefully introduced in dynamic analysis however the model can be an expected numerical tool to simulate not only static problems but also dynamic problems including brittle failure.

## 4 CONCLUSION

In this paper, two lattice spring connecting structures for modeling of the isotropic elastic continuum are compared. The purpose of the discrete modeling is to simulate wave propagation and brittle failure of rock-like materials. The results of the plate with a crack tip demonstrate that the model accurately represents the stress intensity factor and the damping constant should be carefully set to simulate the failure surface development. The second numerical example for the wave propagation shows that the geometry of the discrete lattice structure is important to model the dispersion of wave. Because of the simple material characteristic used in this paper, the simulations only qualitatively represent the behavior of the material. More realistic and quantitative results can be given if inhomogeneity and discontinuity of rock-like materials are introduced.

## ACKNOWLEDGEMENTS

This work is partly supported by Japanese Society for the Promotion of Sciences (JSPS), Grant-in-Aid for Science Research, No.17K06554.

## PREFERENCES

Nishimura, T., Fumimura, K., Kohno, M. & Mitsuhashi, D. 2016. 3D Distinct Element-Based Model for Deformation and Failure of Rock, *Proceedings of 2016 ISRM International Symposium - 9th Asian Rock Mechanics Symposium,* PO4-P74.

Okamura, H. 1976. *Introduction of Linear Elastic Fracture Theory*: 112–118. Tokyo. Baihukan (in Japanese).

Richard, J.B. & Leo, R. 1988. Note on a random isotropic granular material with negative Poisson's ratio, *International Journal of Engineering Science*, 26(4), 373–383.

Walton, K. 1987. The effective elastic moduli of a random packing of spheres, *Journal of the Mechanics and Physics of Solids*, 35(2), 213–226.

Zhao, G.F., Fang, J. & Zhao, J., 2011, A 3D distinct lattice spring model for elasticity and dynamic failure, *International Journal for Numerical and Analytical Methods in Geomechanics*, 35(8), 859–885.

*Rock Dynamics – Experiments, Theories and Applications – Li, Li & Zhang (Eds)*
*© 2018 Taylor & Francis Group, London, ISBN 978-0-8153-9667-3*

# Analysis of elastic wave attenuation in different rock samples

X.L. Liu, G.Y. Zhao, J.H. Cui, X.B. Li & Q. Guo
*School of Resources and Safety Engineering, Central South University, Changsha, China*

ABSTRACT: The attenuation characteristics of elastic wave propagation in granite, marble, red sandstone, and limestone were studied utilizing the PCI-2 acoustic emission system with a lead-break test and automated sensor test (AST) function. The results showed that the attenuation of amplitude was faster when the source was within a certain distance from the sensor: the attenuation became slower as the distance from the source increased. The peak frequencies of the signals in granite and red sandstone were higher when the source was within the faster amplitude attenuation distance, and rapidly reduced as the source moved beyond the distance at a certain extent. However, the peak frequencies of the signals in marble and limestone remained unchanged. The primary factor influencing the attenuation of elastic wave is the density of mineral particles within the rock; the second factor is the development of structures within the rock, such as joints and stratification.

## 1 INTRODUCTION

During elastic wave propagation, its energy can be consumed by geometrical diffusion, material absorption, and scattering. Therefore, parameters of an elastic wave, such as amplitude and frequency, decrease with increasing propagation distance, which is called elastic wave attenuation (Hardy 2003). The degree of attenuation in elastic wave is closely related to the propagating medium, especially in rock materials with heterogeneous internal constructions that determine the attenuation characteristics.

Many scholars have carried out a series of researches on attenuation characteristics of seismic waves in rock masses. It is considered that the amplitude attenuation of seismic wave is closely related to the quality factors of stratum, seismic velocity, and frequency, which are affected by friction, fluid flow, viscosity, and diffusion. The attenuations of P- and S-waves are different (Futterman 1962, Toksoz et al. 1979, White 1975). The frequency characteristics of micro-seismic signals are studied by wavelet transform and window Fourier transform. Four different variation trends of frequency have been identified (Li et al. 2008). In fact, earthquakes, micro-seismic events, and acoustic emission are all external appearances of released elastic energy of rupture in a rock mass: the only difference is their scale of rupture.

Many researches are focused on the attenuation of acoustic emission signals due to the operability of such tests in a laboratory. Vinagradov (Vinagradov 1957, Vinagradov 1962) founded two types of acoustic emission signals (durative and attenuative-type signals), based on his research in field and laboratory tests. These two typical signals obviously derived from different fracture modes. Bucheim (Bucheim 1958) pointed out that the acoustic emission signals generated from a rock sample by shear fractures were characterized by short duration time and wide frequency spectra, whereas those generated by tensile fractures had long duration time and a narrow frequency spectrum. In addition, research has focused on theoretical wave equation analysis and amplitude variation of the constitutive equations of acoustic emission during propagation (Liu et al. 2012, Zou et al. 2004).

Elastic wave attenuation in rock has a strong relationship with the internal structure and composition of rock, so how this attenuation is affected by rock types and the ways in which the parameters of elastic wave signals change as propagation progresses are worthy of discussion. Given this, the lead-break test and the automated sensor test (AST) function of an acoustic emission instrument were used to study the attenuation characteristics of elastic waves in four different types of rock materials: granite, marble, sandstone and limestone. The relationship between the elastic wave attenuation and the microscopic composition of rocks is discussed.